2D/4D marker-free tumor tracking using 4D CBCT as the reference image

Mengjiao Wang[1,2]**, Gregory C Sharp**[2]**, Simon Rit**[3]**, Vivien Delmon**[3] **and Guangzhi Wang**[1]

[1] Department of Biomedical Engineering, School of Medicine, Tsinghua University, Beijing, People's Republic of China
[2] Department of Radiation Oncology, Massachusetts General Hospital, Boston, MA, USA
[3] Creatis Medical Imaging Research Center, University of Lyon, Lyon, France

E-mail: gcsharp@partners.org

Abstract

Tumor motion caused by respiration is an important issue in image-guided radiotherapy. A 2D/4D matching method between 4D volumes derived from cone beam computed tomography (CBCT) and 2D fluoroscopic images was implemented to track the tumor motion without the use of implanted markers. In this method, firstly, 3DCBCT and phase-rebinned 4DCBCT are reconstructed from cone beam acquisition. Secondly, 4DCBCT volumes and a streak-free 3DCBCT volume are combined to improve the image quality of the digitally reconstructed radiographs (DRRs). Finally, the 2D/4D matching problem is converted into a 2D/2D matching between incoming projections and DRR images from each phase of the 4DCBCT. The diaphragm is used as a target surrogate for matching instead of using the tumor position directly. This relies on the assumption that if a patient has the same breathing phase and diaphragm position as the reference 4DCBCT, then the tumor position is the same. From the matching results, the phase information, diaphragm position and tumor position at the time of each incoming projection acquisition can be derived. The accuracy of this method was verified using 16 candidate datasets, representing lung and liver applications and one-minute and two-minute acquisitions. The criteria for the eligibility of datasets were described: 11 eligible datasets were selected to verify the accuracy of diaphragm tracking, and one eligible dataset was chosen to verify the accuracy of tumor tracking. The diaphragm matching accuracy was 1.88 ± 1.35 mm in the isocenter plane and the 2D tumor tracking

accuracy was 2.13 $\pm$ 1.26 mm in the isocenter plane. These features make this method feasible for real-time marker-free tumor motion tracking purposes.

1 Introduction

In image-guided thoracic and abdominal radiotherapy, respiratory motion remains an important challenge. Many approaches have been developed to track tumor motion in real-time, and these methods can be divided into two major categories: methods with implanted markers and marker-free tracking methods. Methods with implanted markers are usually developed to track the markers using fluoroscopy or magnetic tracking systems. They provide accurate tracking results (Seiler *et al* 2000, Sharp *et al* 2004, Tang *et al* 2007) but may not be widely applied because of the risk of complications, such as pneumothoraces. An alternative approach is the marker-free method (Arimura *et al* 2009, Rottmann *et al* 2010, Teo *et al* 2012, Richter *et al* 2010, Aristophanous *et al* 2010, Berbeco *et al* 2005, Cui *et al* 2007, Gendrin *et al* 2012, Hugo *et al* 2010, Lewis *et al* 2010, Lin *et al* 2009, Rohlfing *et al* 2005, Schweikard *et al* 2005, Xu *et al* 2008, Yang *et al* 2012, Gottlieb *et al* 2010). One variation of this method is the use of an electronic portal imaging devices (EPID) image to track the 2D position of the tumor (Arimura *et al* 2009, Rottmann *et al* 2010, Teo *et al* 2012, Richter *et al* 2010, Aristophanous *et al* 2010). While this method is attractive because it reduces the imaging dose to the patient, it is limited by the field-of-view and the poor quality of the EPID images. A perhaps simpler approach is to use fluoroscopic images to track the tumor. After digitally reconstructed radiograph (DRR) images are generated from a 3D volume, they are used as templates for real-time tracking. The registration between templates and fluoroscopic projections to calculate the tumor position in the incoming image has been well established (Berbeco *et al* 2005, Cui *et al* 2007, Gendrin *et al* 2012, Hugo *et al* 2010, Lewis *et al* 2010, Lin *et al* 2009, Rohlfing *et al* 2005, Schweikard *et al* 2005, Xu *et al* 2008, Yang *et al* 2012). Templates can be constructed from different sources, most commonly pre-treatment fluoroscopy (Berbeco *et al* 2005, Cui *et al* 2007, Lin *et al* 2009, Xu *et al* 2008) or simulation CT (Gendrin *et al* 2012, Hugo *et al* 2010, Lewis *et al* 2010, Rohlfing *et al* 2005, Schweikard *et al* 2005, Yang *et al* 2012). Template matching usually involves 2D–2D matching (Berbeco *et al* 2005, Cui *et al* 2007, Lin *et al* 2009, Xu *et al* 2008) or 2D–3D matching (Gendrin *et al* 2012, Hugo *et al* 2010, Lewis *et al* 2010, Rohlfing *et al* 2005, Schweikard *et al* 2005, Yang *et al* 2012), and is usually performed over all breathing phases to identify the best match. This process can be called 2D/4D matching, and has been used to track tumors for both planar fluoroscopy (Berbeco *et al* 2005, Cui *et al* 2007, Lin *et al* 2009, Xu *et al* 2008) and rotational cone beam computed tomography (CBCT) projections (Gendrin *et al* 2012, Hugo *et al* 2010, Lewis *et al* 2010, Rohlfing *et al* 2005, Schweikard *et al* 2005, Yang *et al* 2012).

In this paper, a marker-free tumor tracking method using 2D/4D matching between 4DCBCT and 2D fluoroscopic projection was developed. The motivation of our method is to avoid the disadvantage of implanted markers, and also to avoid the effect of inter-fractional changes in anatomy and breathing pattern between the acquisition of the planning CT and the pre-treatment CBCT. 4DCT is not commonly used at the time of treatment, and daily CBCT is more practical both for radiotherapy and interventional application. Motion measured in

4DCBCT has been shown to be equivalent to motion measured in 4DCT (Gottlieb *et al* 2010). This approach may be applied to image-guided adaptive radiotherapy, as set up for treatment plans customized to a patient's daily tumor motion. It may also be applied to image-guided interventional applications where the treatment plan is generated immediately before the procedure and the target is matched with reference data to conduct interventional treatment.

Because this method relies on template matching, the tumor can be tracked directly if it is visible. Alternatively, in the lower thorax and upper abdomen, the position of the diaphragms can be used as a target surrogate, which will make the visibility of the tumor not strictly required. Using the diaphragm for tumor tracking relies on the assumption that if a patient has the same breathing phase and diaphragm position as the reference 4DCBCT, then the tumor position is the same (Cerviño *et al* 2009).

In this method, firstly, 3DCBCT and phase-rebinned 4DCBCT were reconstructed by cone beam acquisition. The 3D tumor position of each phase can be defined from 4DCBCT volumes. Secondly, 4DCBCT volumes and a 3DCBCT volume were merged to improve the DRR image quality, because DRR images generated from 4DCBCT may suffer from poor quality due to the streak artifacts in the 4DCBCT. Finally, the 2D/4D matching problem was converted into 2D/2D matching between incoming fluoroscopic projection and DRR reference images, because the cone beam acquisition was conducted directly before treatment so the patient position and set up did not change. The gradient difference was used as the matching metric to determine which DRR was the best match. From the matched DRR image and 4D volume, the phase information, diaphragm position and tumor position can be derived. These three major steps, 4DCBCT reconstruction, DRR improvement and 2D/4D matching, are demonstrated in parts 2.2, 2.3 and 2.4 respectively. The performance of this method was verified using 11 out of 16 datasets, including lung and liver applications and one-minute and 2 min CBCT acquisitions. Results suggest that this method is adequate for real-time tumor motion tracking purposes.

2 Method

2.1. Overview of method

The goal of this method is to track a tumor during treatment using 2D/4D matching between 4D volumes derived from CBCT and 2D fluoroscopic projection. The overview of our method is illustrated in figure 1. When the tumor is not easily seen in fluoroscopic projections, the diaphragm is used as a surrogate. After rotational CBCT acquisition, projections are used to reconstruct both a standard 3DCBCT and a phase-rebinned 4DCBCT. The 4DCBCT volumes generally suffer from severe streak artifacts, which affect the image quality of DRRs generated from original 4DCBCT volumes. On the other hand, the 3DCBCT suffers from motion blurring, and is not suitable for the precise localization of a moving target. Therefore, we improve the image quality of the reference DRRs by selectively merging the information in the 3DCBCT and 4DCBCT volumes. Finally, during the treatment, the DRR images generated from improved 4D volumes are used to match incoming 2D fluoroscopic images. The 3D tumor position is then derived from its position in the corresponding 4D volume, as defined before treatment. This method consists of three major steps: 4DCBCT reconstruction, improvement of DRR image quality and 2D/4D matching, which are described in parts 2.2, 2.3 and 2.4 respectively.
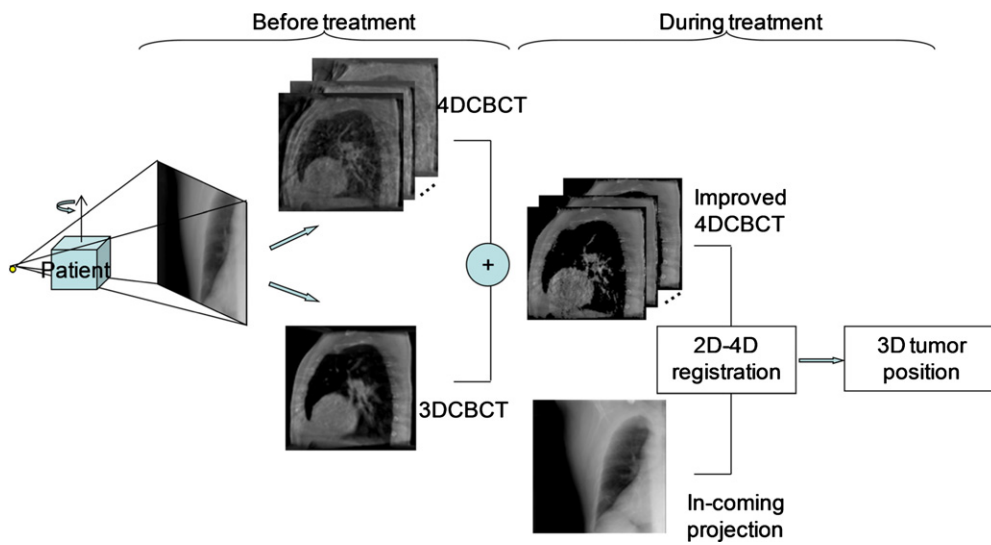
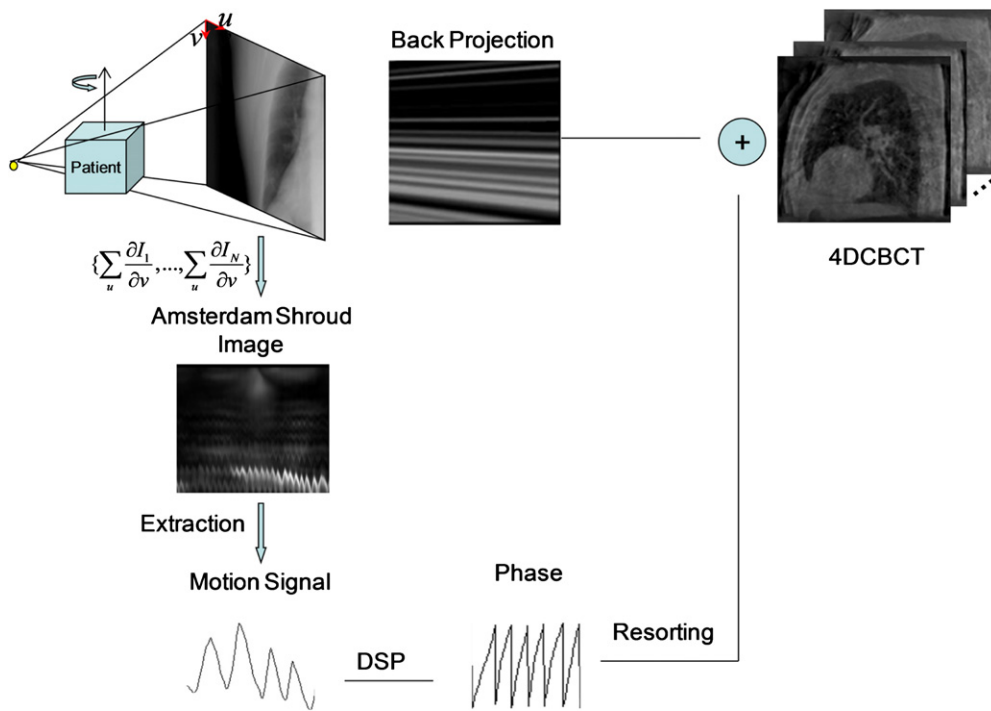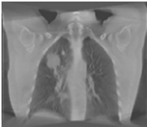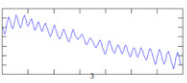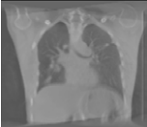**Figure 1.** Diagram of overview for the method.
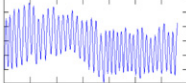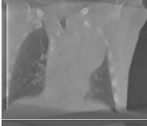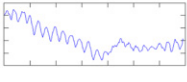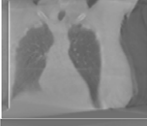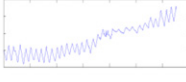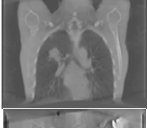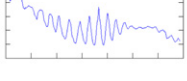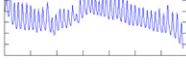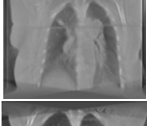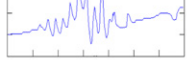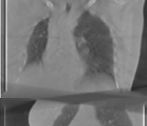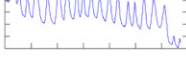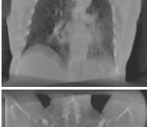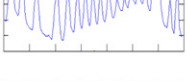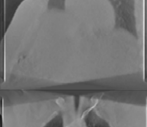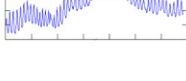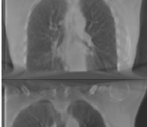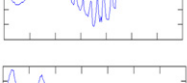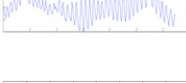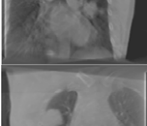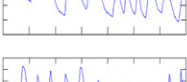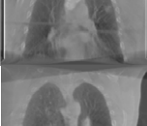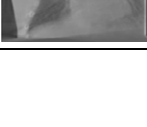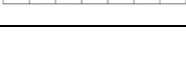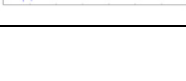
Figure 2. Depiction of the workflow for 4DCBCT reconstruction.

2.2. 4DCBCT reconstruction

The principles of 4DCBCT reconstruction have been demonstrated previously (Sonke *et al* 2005). Here, we used phase-based resorting to reconstruct the 4DCBCT volumes. The work flow is depicted in figure 2. Before treatment, the rotational cone beam projections were

Table 1. Description of 16 datasets.

	3DCBCT	Motion Signal		3DCBCT	Motion Signal
Dataset 1			Dataset 9		
Dataset 2			Dataset 10		
Dataset 3			Dataset 11		
Dataset 4			Dataset 12		
Dataset 5			Dataset 13		
Dataset 6			Dataset 14		
Dataset 7			Dataset 15		
Dataset 8			Dataset 16		

acquired. The motion signal was extracted from raw fluoroscopic projections using the Amsterdam Shroud algorithm, as depicted in figure 2 and as described by Sonke and Rit (Sonke *et al* 2005, Rit *et al* 2012). The Amsterdam Shroud algorithm first calculates the partial derivative of projection along the column direction, assuming the primary diaphragm movement is along the same direction. Then these values are accumulated along each row. By aligning the sequence of Amsterdam Shroud results over all rotational projections, the motion signal was obtained. Once the Amsterdam Shroud image was derived, a column-to-column registration method was used to extract the motion signal. This method was implemented in the reconstruction tool kit (RTK) (Rit *et al* 2013). Overall, the method achieved a good quality motion signal for most patients studied, but its final result does suffer from baseline drifting, which can be seen in table 1.

After the motion signal was extracted, a Hilbert transformation was used to extract the phase of the motion signal. Projections were resorted into eight phase-rebinned subsets, which we describe as early exhale, middle exhale, late exhale, peak exhale, early inhale, middle
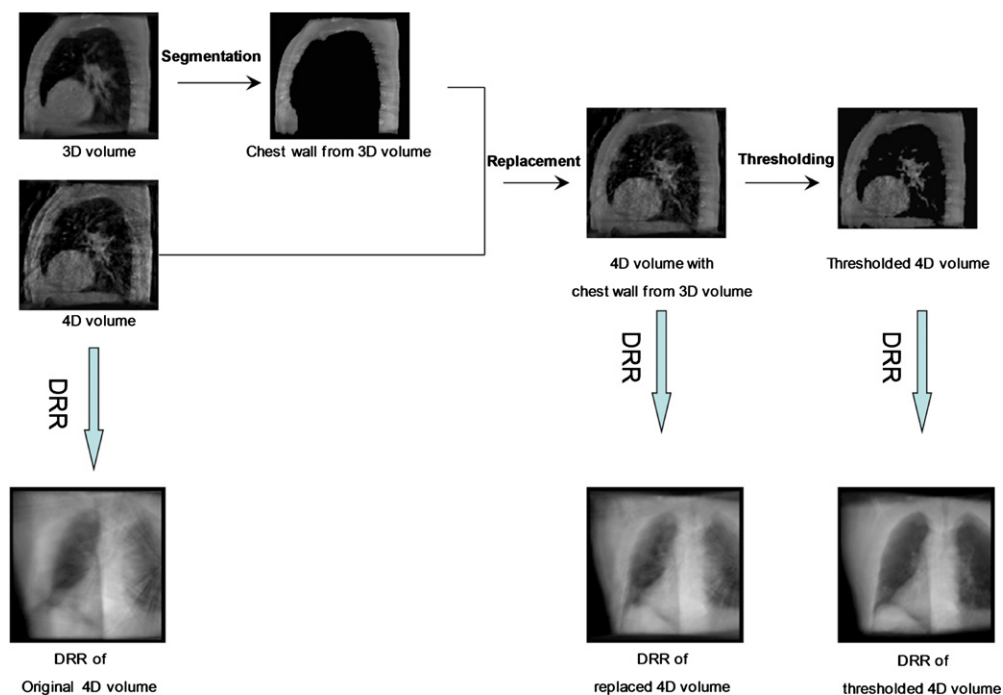
Figure 3. Work flow of DRR quality improvement.

inhale, late inhale and peak inhale, and each subset of projections was used to reconstruct one phase of the 4DCBCT volume. The Hilbert transformation did not work properly for motion signals with a high degree of drift; in these cases, the maxima and minima of the motion signal were extracted, and then the projections were resorted based on the velocity between each maximum and minimum.

2.3. Improvement of DRR image quality generated from a 4D volume

DRR images generated from 4DCBCT volumes suffer from poor image quality due to streak artifacts, which limited their use as a template image for image-guided procedures. Therefore, the image quality of DRR derived from 4DCBCT should be improved.

In our method, rotational CBCT projections were used to create two output images: a phase-rebinned 4D volume and a relatively streak-free 3D volume. These volumes are combined into a composite 4D volume that includes stationary voxels from 3DCBCT and moving voxels from 4DCBCT. Stationary voxels include the chest wall. As explained by Kaneko (Kaneko and Horie 2012), the overall movement of the sternal angle and xiphoid process during quiet breathing is 2.57 ± 1.62 mm and 2.82 ± 1.44 mm, respectively. Therefore we conclude that the movement of the chest wall is small compared to other uncertainties in 4DCBCT, i.e. the diaphragm movement, and the chest wall can be treated as stationary. The voxels with large motion are the soft tissues inside the chest wall, including the lung, heart and abdomen. The procedure for merging the 3D and 4D volumes is depicted in figure 3. First, the chest wall was segmented in the 3D volume, and the segmented result was copied in-place over corresponding voxels in the 4D volume. The purpose of the chest
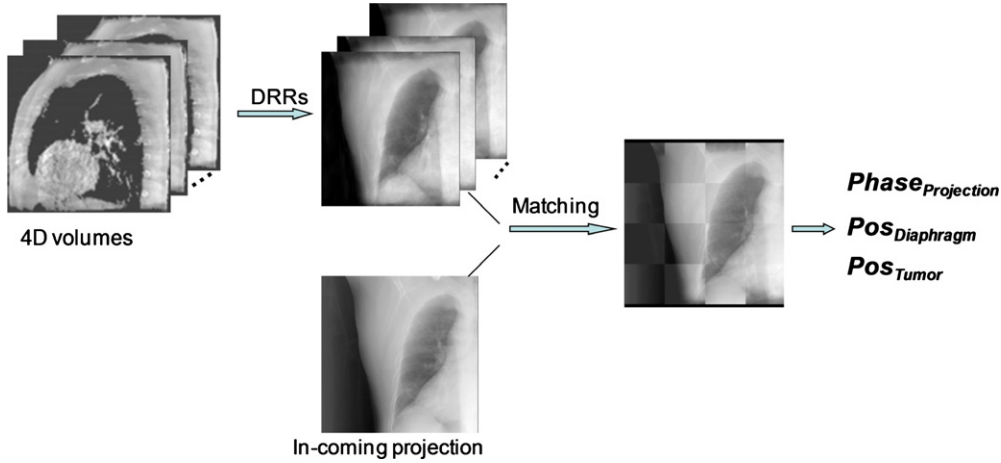
Figure 4. Workflow of 2D/4D matching.

wall replacement is to improve the visibility and consistency of the bony anatomy, while preserving motion information. For generating the DRR, a threshold was applied to remove low-intensity voxels, leaving the chest wall, bony structure, heart, abdomen, tumor and major vessels and bronchi. The purpose of the thresholding is to reduce streak artifacts in the 4D volume, while again preserving motion information present in the lungs and diaphragm. From figure 3, we can see that the DRR images generated from raw 4DCBCT are visually poor because of the streak artifacts. The DRR images computed from the combined 3D and 4D volumes are visually more similar to the original projection images.

2.4. 2D/4D matching

In our work, 2D/4D matching uses the diaphragm position as the matching target. The purpose of 2D/4D matching is to simultaneously determine the phase and offset of each incoming 2D projection relative to the reference 4DCBCT volume. In this way, the 3D tumor position can be derived in real-time. Since the rotational CBCT acquisition was directly conducted before treatment, the patient setup and position are assumed to be very similar in both the CBCT acquisition and treatment. Therefore the registration between the 4D volume and the incoming projection can be simplified to a 2D/2D matching problem between DRR images generated from each phase of the 4D volume and the incoming projection image. The work flow was depicted in figure 4. For our study, 2D/2D matching was performed using the gradient difference metric.

To implement this procedure, four steps are proposed.

(1) Use the known projection geometry of the incoming fluoroscopic image to generate DRR images for each phase of the 4D volume.
(2) Normalize the DRR images and incoming projection image for matching purposes. The normalization method is:

$$V_{\text{output}} = (V_{\text{input}} - \mu)/\sqrt{\sigma} \tag{1}$$

   where μ is the mean value of the input image and σ is the variance of the input image.
(3) Match the DRR images with the incoming projection image based on a region of interest (ROI), which was the diaphragm in our experiments. The ROI was selected as a 10 cm

square with the apex of the diaphragm as the center. The gradient difference was chosen as the metric for 2D/2D matching. Because we merged a 3D and 4D volume and thresholded the high-intensity voxels to generate the DRR images, the intensity of the DRR was not linearly related to the original projection image. For this reason, a gradient-based method is selected for this application. The region containing the diaphragm has a large difference in intensity and matches well using a gradient-based metric. The gradient difference metric is shown in equation (2). It uses $1/(1 + x^2)$ as the pattern intensity to make this metric robust for a thin line structure (Penney *et al* 1998):

$$\text{diff}\,(a) = \sum_{i,j} \frac{A_h}{A_h + \text{diff}H\,(i,\,j)^2} + \sum_{i,j} \frac{A_v}{A_v + \text{diff}V\,(i,\,j)^2} \tag{2}$$

where diff$H$ (i, j) and diff$V$ (i, j) are the horizontal and vertical gradient differences.

$$\text{diff}H\,(i,\,j) = \frac{\partial I_1}{\partial j} - a\frac{\partial I_2}{\partial j} \tag{3}$$

$$\text{diff}V\,(i,\,j) = \frac{\partial I_1}{\partial i} - a\frac{\partial I_2}{\partial i}. \tag{4}$$

A_v and A_h are equal to the variance of diff$V$ and diff$H$. The scaling factor a is set to 1.0. The DRR image with maximum value is selected as the phase of the incoming 2D projection.

(4) The 3D tumor position and diaphragm position can be obtained from the corresponding phase of the 4D volume, based on the tumor position, which has been defined before treatment.

3 Materials

A total of 16 CBCT acquisition datasets were selected as candidates to verify this method. The 3DCBCT reconstructed volume and extracted motion signal for each dataset is shown in table 1. From the initial group, 11 datasets were selected to verify the performance of the diaphragm tracking, and one eligible dataset was chosen to verify the accuracy of the tumor tracking.

The descriptions for each dataset are as follows. Datasets 1 to 8 were acquired using one-minute rotational CBCT acquisitions, while datasets 9 to 16 were 2 min acquisitions. Dataset 11 and 13 demonstrate a liver application, while the remaining datasets demonstrate a lung application. In datasets 3 and 6, we can hardly see the diaphragm, and in datasets 1, 2, 7 and 15, the diaphragms are near the bottom of the image edge. In the remaining datasets, the diaphragms are visible in the lower or middle part of the volume.
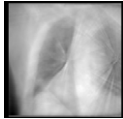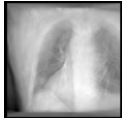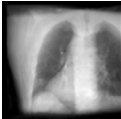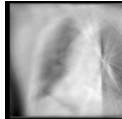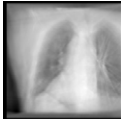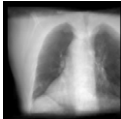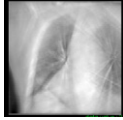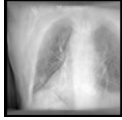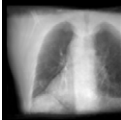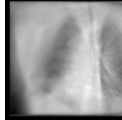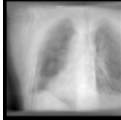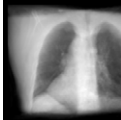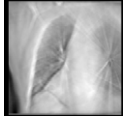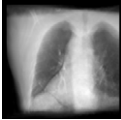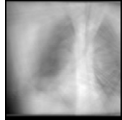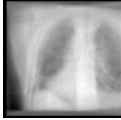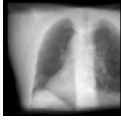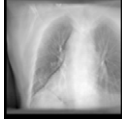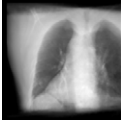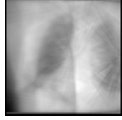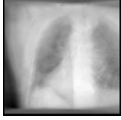
Not all of the datasets presented above are eligible for this method. The eligible datasets were selected based on the following criteria.

(1) Visibility of diaphragm: since the 2D/4D matching method is based on the position of the diaphragm, the diaphragm should be visible in the reconstructed volume.

(2) Regularity of motion signal: the phase-based projection resorting and 2D/4D matching rely on the regularity of the motion signal. Irregular breathing can cause uncertainty to the phase-based projection resorting and may lead to a failure of the diaphragm matching since the diaphragm displacement is unpredictable and may be out of the search range of the templates.

(3) Patient size: a large patient size affects the visibility of the diaphragm in DRR images at gantry angles around the right–left lateral projection, limiting matching accuracy.

Based on these criteria, datasets 3, 4, 6, 13 and 15 (31% of the 16 cases) were excluded.

Table 2. DRR images of eight phases, comparing three different stages of processing.

	DRR of Original 4D	DRR of Replaced 4D	DRR of Thresholded 4D		DRR of Original 4D	DRR of Replaced 4D	DRR of Thresholded 4D
Early Exhale				Early Inhale			
Middle Exhale				Middle Inhale			
Late Exhale				Late Inhale			
Peak Exhale				Peak Inhale			

4 Results

The key steps for this method include 4DCBCT reconstruction, 3D and 4D volumes merging and 2D/4D matching. Results for DRR image quality improvement using merged volumes are presented in part 4.1, and results for 2D/4D matching are presented in part 4.2.

4.1. Results for improvement of DRR image quality

Representative DRR images generated using original, replaced and thresholded 4D volumes are shown in table 2. Here, 'original' 4D volumes refer to the unaltered 4DCBCT volumes. 'Replaced' 4D volumes mean 4D volumes after chest wall voxels were replaced with voxels from the streak-free 3DCBCT volume. 'Thresholded' 4D volumes refer to the 4D volumes after thresholding to remove low-intensity voxels. From table 2, we can see that the image quality of the DRR has improved and is visually more similar to a projection image.

A qualitative assessment of image quality for DRR images was conducted by defining the visibility of major anatomical landmarks in DRR images generated from 'original', 'replaced' and 'thresholded' 4D volumes. Those major anatomical landmarks included the ribs, spine, diaphragm and carina. 'Good', 'Acceptable' and 'Poor' visibility were assigned numeric values of 10, 5 and 0, respectively. The mean value and standard deviation were calculated from four reviewers' assessments for all eight phases of different 4D volumes. The qualitative assessment results for DRR images derived from 'original', 'replaced' and 'thresholded' 4D volumes were presented in table 3. The reviewers were not told which method was used to create the images. From the table, we can see that the visibility of anatomic structures in the DRR was improved by 4D volume modification.

The apex of the ipsilateral diaphragm in AP view DRR images generated from 'original', 'replaced' and 'thresholded' 4D volumes were manually identified to determine whether motion information was preserved during volume processing. This procedure was carried out for four selected datasets: 10, 11, 12 and 16. These datasets were used for this validation
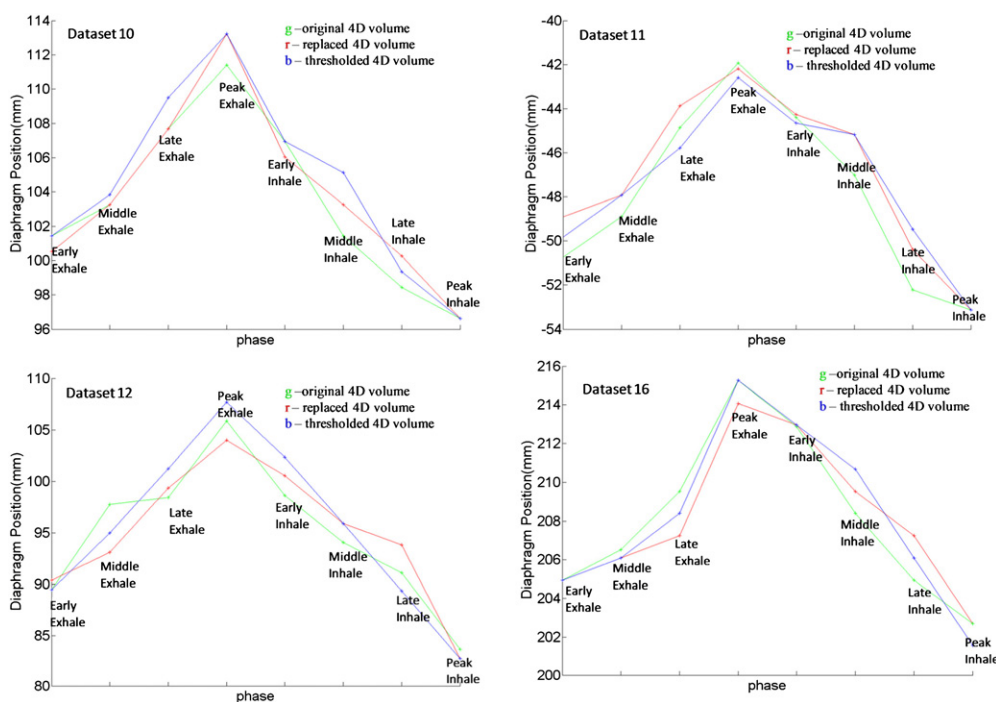
Figure 5. Comparison of diaphragm movement in DRR images generated from different 4D volumes; the green line refers to the motion curves plotted using DRRs generated from original 4D volumes; the red line refers to the motion curves plotted using DRRs generated from replaced 4D volumes; and the blue line refers to the motion curves plotted using DRRs generated from thresholded 4D volumes.

Table 3. Qualitative assessment of image quality for DRRs of orignal, replaced and thresholded 4D volumes based on the visibility of major anatomy. The 'good', 'acceptable' and 'poor' visibilities were assigned numeric values of 10, 5 and 0, respectively. Four reviewers' assessments of all eight breathing phases in multiple patients are combined.

	Ribs	Spine	Diaphragm	Carina
Original volume	1.2 ± 0.7	1.8 ± 1.0	2.3 ± 1.0	0.7 ± 0.7
Replaced volume	3.4 ± 2.7	4.1 ± 2.4	5.4 ± 1.2	1.6 ± 1.8
Thresholded volume	7.2 ± 3.9	7.6 ± 2.3	8.0 ± 1.7	5.7 ± 2.4

procedure because the diaphragm was most clearly visible in the 'original' or 'replaced' DRR images, and therefore we felt confident about manual identification of its position.

The result is presented in figure 5. We can see that the motion of the diaphragm in all four DRR datasets is consistent throughout the processing, in terms of both amplitude and pattern. Therefore, we conclude that the motion information was well-preserved using this method.

4.2. Results for 2D/4D matching

The purpose of 2D/4D matching is to align the incoming 2D fluoroscopic projection and DRR images of difference phases based on the position of diaphragm. This method was used to

Table 4. Accuracy of phase determination using a projection-DRR matching method for eligible datasets. The numbers '0', '1', '2', '3' and '4' mean that the difference between the phases determined by the 2D/2D matching method and the phases assigned by phase-based projection resorting are 0 phases, 1 phase, 2 phases, 3 phases and 4 phases, respectively.

Phase differences	0	1	2	3	4
Dataset 1	58.26%	25.22%	6.67%	5.80%	4.06%
Dataset 2	60.29%	21.40%	9.59%	7.27%	1.45%
Dataset 5	63.77%	22.03%	8.41%	4.64%	1.16%
Dataset 7	55.59%	19.12%	13.53%	5.98%	5.78%
Dataset 8	65.29%	19.71%	5.59%	6.47%	2.94%
Dataset 9	67.66%	17.66%	9.84%	3.59%	1.25%
Dataset 10	69.22%	9.22%	9.60%	7.44%	4.52%
Dataset 11	61.09%	32.34%	3.75%	2.19%	0.63%
Dataset 12	59.53%	14.22%	10.59%	9.06%	6.59%
Dataset 14	59.06%	33.44%	4.06%	2.66%	0.78%
Dataset 16	70.38%	18.02%	9.33%	1.08%	1.18%
Average	62.74%	21.12%	8.27%	5.10%	2.77%
Cumulative	62.74%	83.86%	92.13%	97.23%	100.00%

determine the phase and diaphragm position, and eventually the tumor position. Results for phase determination, diaphragm position accuracy and 2D tumor tracking accuracy are each presented.

To validate the phase determination, incoming fluoroscopic projections were selected from the dataset used for CBCT reconstruction. The 2D/2D matching method between DRR images of different phases and incoming projections was applied. Accuracy of the phase determination is evaluated by assigning a number from 1 to 8 for each phase and subtracting the phase number modulo 8. The result for each dataset is shown in table 4. In this table, the numbers '0', '1', '2', '3' and '4' mean that the difference between the phases determined by the 2D/2D matching method and the phases assigned by phase-based projection resorting are 0 phases, 1 phase, 2 phases, 3 phases and 4 phases, respectively.

Phase information can be ambiguous, especially with the irregular breathing motion, and small errors in phase are probably less important than large errors. For this reason, we calculate the cumulative percentage of images with different degrees of mismatch. In our results, we found that 92.13% of the images match within two phases, which gives confidence in the phase selection stage of the 2D/2D matching method.

To validate the 2D/2D matching accuracy, the apex of the diaphragm in the matched DRR image and the original projection were manually identified, and the distance between these two positions in the isocenter plane was calculated. Projection images at typical gantry angles were selected, including gantry angles 0, 45, 90, 135, 180, 225, 270 and 315. The results are presented in table 5. From table 5, we can see that the diaphragm matching error is 1.88 ± 1.35 mm, which verifies the effectiveness of the 2D/2D matching method.

To establish the benefit of the DRR image quality improvement, we carried out an experiment to evaluate the diaphragm matching accuracy using the original DRR image. The result was 2.73 ± 2.50 mm with a failure rate of 5.7%. In comparison with the diaphragm matching using the improved DRR image, we can see that the improved DRR images had better accuracy.

To verify the sensitivity of the ROI selection, we compared the diaphragm matching result using the 10 cm ROI with a smaller and a larger ROI. A 5 cm square around the diaphragm

Table 5. Accuracy of diaphragm matching between DRR images and incoming projections for different datasets.

	Mean value (mm)	Standard deviation (mm)	Failure cases (dist > 5.0 mm)
Dataset 1	0.76	0.55	0
Dataset 2	1.35	0.58	0
Dataset 5	2.58	1.62	0
Dataset 7	2.18	1.48	0
Dataset 8	3.32	1.38	0
Dataset 9	1.89	1.65	0
Dataset 10	2.37	2.19	1
Dataset 11	1.19	1.01	0
Dataset 12	1.59	1.18	0
Dataset 14	1.85	1.95	1
Dataset 16	1.57	1.28	0
Overall	1.88	1.35	2/88 (2.23%)

Table 6. Comparison of the diaphragm matching accuracy using different ROI selections: 5 cm square, 10 cm square and the whole image region.

ROI selection	Diaphragm matching accuracy (mm)
5 cm square	2.89 ± 2.25
10 cm square	1.88 ± 1.35
Whole image region	2.91 ± 1.85

apex was used as the smaller ROI, whereas the whole image region was used as the larger ROI. For the 5 cm ROI, the diaphragm matching accuracy was 2.89 ± 2.25 mm with a failure rate of 7.95%. For the whole image region, the result was 2.91 ± 1.85 mm with a failure rate of 3.41%. The diaphragm matching accuracies for different ROI selections are summarized in table 6.

To visually assess the accuracy of the tumor tracking, dataset 7 was selected for this purpose based on the following criteria: (1) the tumor should be visible in the DRR and projection images; (2) the tumor should be in the lower thorax so that the tumor motion is highly correlated with respiration. Although the visibility of the tumor in 2D images is not required for tracking, it is used for verification. To verify the 2D tumor tracking accuracy, we manually identified the center of the tumor in both the DRR image and in the incoming fluoroscopic projection image, and then compared the distance between the tumor centers in the isocenter plane. The distance was 2.13 ± 1.26 mm, which we feel is acceptable for diaphragm-based tumor tracking.

In our implementation, 2D/2D matching took 0.48 s to compute for each incoming image. The computer used here has an Intel Xeon (R) E5503 at 2.00 GHz and 12.0 GB installed memory. Therefore we conclude that this method can be sufficient for real-time tracking. To achieve real-time performance, GPU acceleration or the selection of an ROI can be applied.

5. Discussion

A method of 2D/4D matching was implemented for marker-free tumor motion tracking. Firstly, the phase-rebinned 4DCBCT and 3DCBCT were reconstructed using rotational cone
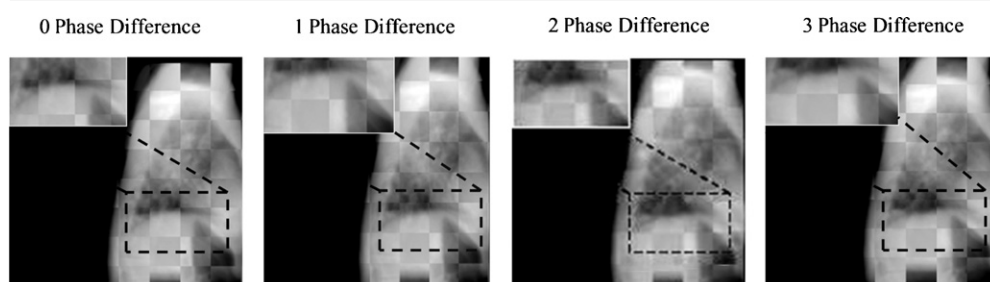
Figure 6. Ambiguity between breathing phase and amplitude.

beam acquisition. Secondly, the 4DCBCT and 3DCBCT were merged to improve the DRR image quality. Finally, the DRR images and incoming projection were matched to determine the breathing phase, diaphragm position and tumor position at that time of incoming projection acquisition.

The goal of our method is to avoid the complications of implanted markers, and also to avoid the effect of inter-fractional changes in anatomy and breathing pattern between the planning CT and pre-treatment CBCT. Because the matching can use the diaphragm position as a target surrogate, the visibility of the tumor in the 2D image is not strictly required. The 2D/4D matching problem is reduced to phase selection and 2D/2D matching, which reduces the computation time.

Regarding the phase assignment based on 2D/2D matching between DRR images and the projection image, we define the phase assignment as being correct if the cumulative accuracy is between '0' and '2' in table 4, for which we achieved correct phase selection for 92.13% of the images. This criterion is admittedly generous, to reflect the ambiguity between phase and amplitude caused by baseline drift. Even for patients under quiet respiration, the inhale and exhale positions vary over time. An example of this effect is shown in figure 6. Each subfigure was generated by applying the checkerboard pattern between the projection image and the corresponding DRR. From figure 6, we can see that DRRs with phase differences between 0 and 2 can all be considered acceptable in terms of providing a good reference for matching. This explains our choice of cumulative accuracy from '0' to '2' in table 4.

Comparing the rotational CBCT acquisition of one minute and two minutes, we were surprised to find that the performance for datasets with 2 min' acquisition was not obviously better than for datasets with 1 min acquisition, regarding the accuracy for phase assignment and diaphragm matching. Therefore, a standard 1 min CBCT acquisition can be performed to avoid a longer acquisition time.

Our results show that the improved DRR image quality increases the accuracy of diaphragm matching. The reason for this is probably because of the severe streak artifacts in the original DRR image. These streaks cause large image gradients, which affect the calculation of the gradient difference, leading to decreased 2D/4D matching accuracy.

To verify the sensitivity of ROI selection, we compared the diaphragm matching result using three different ROI strategies. From table 6, we can see that the 10 cm ROI has the best diaphragm matching accuracy. The reason may be that in the 10 cm square ROI, the entire diaphragm, as well as portions of the spine and chest wall, are included. However, in the smaller ROI, only a portion of the diaphragm region is included, and in the larger ROI, the scanning bed and other static regions are included. Therefore, the ROI size does affect the calculation of the gradient difference and the 2D/4D matching.

Cycle-to-cycle variation has not been considered in this paper. Patients with irregular breathing patterns that cause a failure in 4D resorting were considered ineligible and were excluded. However, breathing variation may also affect 2D/4D matching. One might address this by assigning an impact factor to each 4DCBCT volume based on the matching result, and then use a voting or interpolation method to derive the tumor position. In addition, we should consider carefully a preoperative selection method that can identify which patients are eligible for this method. We have retrospectively identified the importance of diaphragm visibility, breathing regularity and patient size, but establishing concrete metrics for eligibility remains for future studies.

6. Conclusion

A 2D/4D matching method was developed to track tumor motion during treatment using a 4DCBCT as a reference image. The performance of this method was verified based on the accuracy of phase assignment and 2D/2D matching. Our results suggest that this method may be sufficient for real-time tumor motion tracking in a subset of patients. This marker-free tumor motion tracking method can account for the inter-fractional changes in anatomy and breathing pattern between the acquisition of the planning CT and actual treatment. Since the matching method can use diaphragm position as a surrogate, the visibility of the tumor in the 2D projection images is not strictly required.

Acknowledgments

References   Q3

Arimura H *et al* 2009 Computerized method for estimation of the location of a lung tumor on EPID cine images without implanted markers in stereotactic body radiotherapy *Phys. Med. Biol.* **54** 665–77

Aristophanous M, Rottmann J, Park S-J, Nishioka S, Shirato H and Berbeco R I 2010 Image-guided adaptive gating of lung cancer radiotherapy: a computer simulation study *Phys. Med. Biol.* **55** 4321–33

Berbeco R I, Mostafavi H, Sharp G C and Jiang S B 2005 Towards fluoroscopic respiratory gating for lung tumours without radiopaque markers *Phys. Med. Biol.* **50** 4481–90

Cerviño L I, Chao A K Y, Sandhu A and Jiang S B 2009 The diaphragm as an anatomic surrogate for lung tumor motion *Phys. Med. Biol.* **54** 3529–41

Cui Y, Dy J G, Sharp G C, Alexander B and Jiang S B 2007 Multiple template-based fluoroscopic tracking of lung tumor mass without implanted fiducial markers *Phys. Med. Biol.* **52** 6229–42

Gendrin C *et al* 2012 Monitoring tumor motion by real time 2D/3D registration during radiotherapy *Radiother. Oncol.* **102** 274–80

Gottlieb K L, Hansen C R, Hansen O, Westberg J and Brink C 2010 Investigation of respiration induced intra- and inter-fractional tumour motion using a standard Cone Beam CT *Acta. Oncol.* **49** 1192–8

Hugo G D, Liang J and Yan D 2010 Marker-free lung tumor trajectory estimation from a cone beam CT sinogram *Phys. Med. Biol.* **55** 2637–50

Kaneko H and Horie J 2012 Breathing movements of the chest and abdominal wall in healthy subjects *Respir. Care.* **57** 1442–51

Lewis J H, Li R, Watkins W T, Lawson J D, Segars W P, Cerviño L I, Song W Y and Jiang S B 2010 Markerless lung tumor tracking and trajectory reconstruction using rotational cone-beam projections: a feasibility study *Phys. Med. Biol.* **55** 2505–22

Lin T, Cerviño L I, Tang X, Vasconcelos N and Jiang S B 2009 Fluoroscopic tumor tracking for image-guided lung cancer radiotherapy *Phys. Med. Biol.* **54** 981–92

Penney G P, Weese J, Little J A, Desmedt P, Hill D L and Hawkes D J 1998 A comparison of similarity measures for use in 2-D-3-D medical image registration *IEEE Trans. Med. Imaging* **17** 586–95

Richter A, Wilbert J, Baier K, Flentje M and Guckenberger M 2010 Feasibility study for markerless tracking of lung tumors in stereotactic body radiotherapy *Int. J. Radiat. Oncol. Biol. Phys.* **78** 618–27

Rit S, Oliva M V, Sebastien B, Labarbe R, Sarrut D and Sharp G C 2013 The reconstruction Toolkit (RTK), an open source cone-beam CT reconstruction toolkit based on the Insight Toolkit (ITK) *Int. Conf. on the use of Computer in Radiation Therapy*   **Q4**

Rit S, van Herk M, Zijp L and Sonke J-J 2012 Quantification of the variability of diaphragm motion and implications for treatment margin construction *Int. J. Radiat. Oncol. Biol. Phys.* **82** e399–407

Rohlfing T, Denzler J, Grässl C, Russakoff D B and Maurer C R 2005 Markerless real-time 3-D target region tracking by motion backprojection from projection images *IEEE Trans. Med. Imaging* **24** 1455–68

Rottmann J, Aristophanous M, Chen A, Court L and Berbeco R 2010 A multi-region algorithm for markerless beam's-eye view lung tumor tracking *Phys. Med. Biol.* **55** 5585–98

Schweikard A, Shiomi H and Adler J 2005 Respiration tracking in radiosurgery without fiducials *Int. J. Med. Robot.* **01** 19–27

Seiler P G, Blattmann H, Kirsch S and Muench R K S C 2000 A novel tracking technique for the continuous precise measurement of tumour positions in conformal radiotherapy *Phys. Med. Biol.* **45** N103–5

Sharp G C, Jiang S B, Shimizu S and Shirato H 2004 Tracking errors in a prototype real-time tumour tracking system *Phys. Med. Biol.* **49** 5347–56

Sonke J-J, Zijp L, Remeijer P and van Herk M 2005 Respiratory correlated cone beam CT *Med. Phys.* **32** 1176–86

Tang X, Sharp G C and Jiang S B 2007 Fluoroscopic tracking of multiple implanted fiducial markers using multiple object tracking *Phys. Med. Biol.* **52** 4081–98

Teo P, Crow R, Van Nest S and Pistorius S 2012 Tracking a phantom's lung tumour target using optical flow algorithm and electronic portal imaging devices *IEEE Int. Conf. on Imaging Systems and Techniques Proc.* pp 51–6

Xu Q, Hamilton R J, Schowengerdt R A, Alexander B and Jiang S B 2008 Lung tumor tracking in fluoroscopic video based on optical flow *Med. Phys.* **35** 5351–9

Yang Y, Zhong Z, Guo X, Wang J, Anderson J, Solberg T and Mao W 2012 A novel markerless technique to evaluate daily lung tumor motion based on conventional cone-beam CT projection data *Int. J. Radiat. Oncol. Biol. Phys.* **82** e749–56

QUERIES

Page 2
Q1
Author: Please provide kewords relevant to your paper.

Q2
Author: Please be aware that the color figures in this article will only appear in color in the Web version. If you require color in the printed journal and have not previously arranged it, please contact the Production Editor now.

Page 14
Q3
Author: Please check the details for any journal references that do not have a blue link as they may contain some incorrect information. Pale purple links are used for references to arXiv e-prints.

Page 15
Q4
Author: Please provide page range in reference 'Rit *et al* 2013'.